In the first one, real-time application torque T, angular wheel speeds ω_w, and EV velocity v, obtained from BBSi are managed by the front-end Slip Processing block. Here, longitudinal wheel slip λ (9) and application torque derivative $dT/d\lambda$ with respect to slip are calculated.

In the second stage, generation of actuating braking torque T^* dependently of the pedal displacement (driver's setpoint) T_B^* and application torque derivative $dT/d\lambda$ is produced by the FLC referring to expert's knowledge due to system complexity and high nonlinearity.

Finally, the output stage algorithmically distributes actuating braking torque T^* between front and rear wheels at a fixed ratio [21] and allocates it between FB and EB based on the real-time *SOC*, voltage of HES, and permissible EB current.

The demanded EB and FB commands T_E^*, T_F^* generated by ECU are directed to the appropriate BBS interfaces. Electric current I_E recharges HES from EB whereas the pressure signal p_F adjusts FB. Braking will complete as the driver releases the pedal or the vehicle comes to stop.

Fig. 3 demonstrates the performance algorithm of the torque allocation stage.

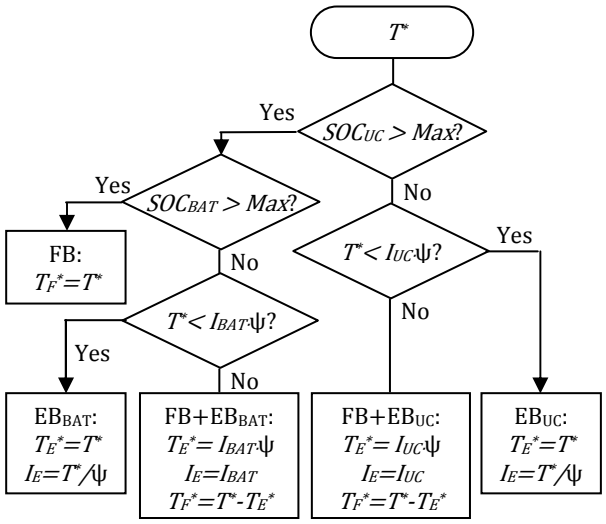

Fig. 3. Torque allocation algorithm.

Here, once ECU detects the actuating torque request T^*, EB is activated and either EB_{UC} or EB_{BAT} runs. The FB torque does not appear until any of *SOC* levels exceeds permissible overcharging barriers (*Max*) or electric motor produces maximal power. Since motor torque becomes insufficient, the ECU runs FB and EB together ($FB+EB_{UC}$ or $FB+EB_{BAT}$). In the case when both *SOC* levels overcome their boundaries, the sole FB is used due to recuperation impossibility.

The main benefit of this algorithm is in inclusion of recuperation in all braking scenarios, even in heavy braking with ABS.

6. Design of the Fuzzy Logic Converter

The FLC target is to derive actuating braking torque needed for slowing down the EV inside an acceptable adhesion-slip region μ-λ. The controller with multiple inputs and single output has been designed. Here, two input numerical variables (crisps) are used – driver's setpoint T_B^* and application torque derivative $dT/d\lambda$ with respect to slip λ. The Sugeno-style inference mechanism is applied to transform every input crisp into a separate fuzzy pair consisting of an element in universe of discourse and an appropriate membership function (MF). Estimated actuating torque T^* is coming from the FLC output. Using the weighted average defuzzification method, this linguistic singleton signal is then turned back to the real-world output crisp.

The torque T_B^* input and torque derivative $dT/d\lambda$ input have four MFs notated as Z (Zero), S (Small), M (Middle), and L (Large). In Fig. 4, fuzzy sets for the linguistic variables are represented. The MFs have triangle and trapezoidal shapes suitable for braking management and experts training.

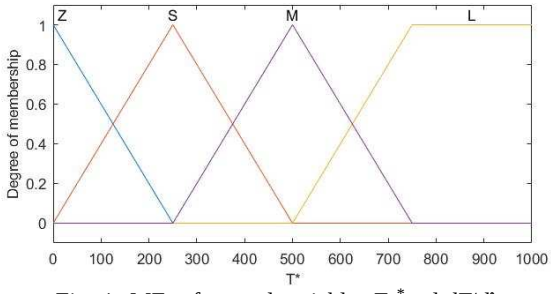

Fig. 4. MFs of control variables T_B^* and $dT/d\lambda$.

The inference engine with "If–Then" modus ponens converts the fuzzy input sets to the fuzzy output set using the rule base of 16 rules represented in Table I.

TABLE I. FLC RULE BASE

Torque derivative $dT/d\lambda$	Output torque T^* at input T_B^*			
	Z	*S*	*M*	*L*
Z	Z	Z	Z	Z
S	Z	S	S	S
M	Z	S	M	M
L	Z	M	M	L

The resulting input-output FLC surface is plotted in Fig. 5.

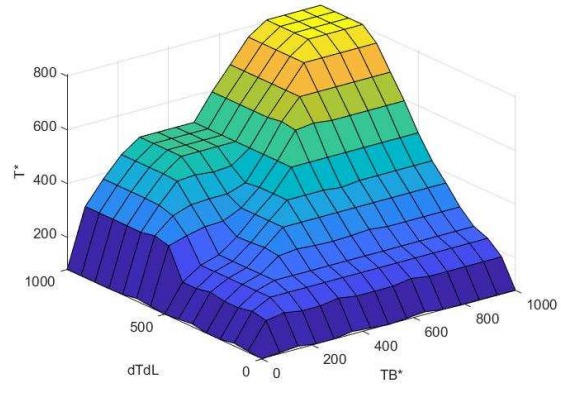

Fig. 5. Input-output FLC surface.

7. Results and Discussion

In the initial part of this research published in [10], the core of the offered methodology was validated with the help of the hardware-in-the-loop electro-hydraulic testbed from ZF TRW Automotive (Koblenz, Germany) driven by the vehicle-oriented software IPG CarMaker® (Karlsruhe, Germany), which ran the ABS imitator of an

electric sport utility vehicle. Using an original FLC, that system successfully recognises road surfaces and provides blended braking.

Mass of the studied sport utility vehicle was of 2117 kg and wheel radius of 0.2 m. It was assumed that the EV is moving in a straight-line manoeuvre at 100 km/h fed by the switch-reluctance motor with maximal permissible torque of 200 Nm, speed 157 rad/s, and 2.1 kgm^2 inertia connected to the wheel imitator through the gear of 10.5 ratio. Due to the gear, peak torque on the wheel at heavy braking approached 2000 Nm and wheel angular speed – 15 rad/s. Aerodynamic and climbing factors were neglected in that study.

In Fig. 6, two braking diagrams obtained in [10] are shown: wheel velocities of the front left (*FL*), front right (*FR*), rear left (*RL*), and rear right (*RR*) wheels, appropriately, that follow the vehicle longitudinal velocity *v* in Fig. 6 (a), and EB and FB wheel torque curves in Fig. 6 (b). As EB torque is not enough to retain optimal slip, the ECU requests additional FB torque. At the end of slowing down, recuperation turns off, and FB completes braking alone.

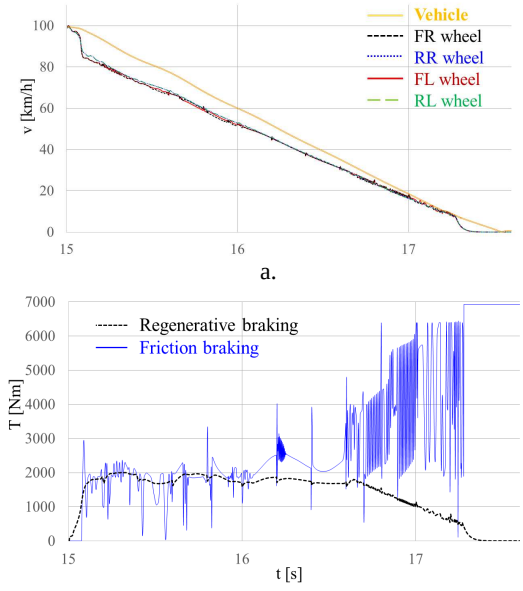

Fig. 6. Hardware-in-the-loop experimental diagrams: a) vehicle and wheel velocities; b) torque.

Alongside the number of positive outcomes, the evident chattering phenomenon at low velocity is seen in the torque curves. In fact, three interconnected reasons may explain its appearance. First, increase of friction due to its static fraction in (6) when the vehicle moves slowly and several wheels tends to slip. Second, air friction (4) is ignored. Third, as at low velocity EB ceases and FB finalises braking alone, no torque stabilisation exists at that moment. Torque oscillations demonstrate that the simplified drive model used in [10] could not ensure proper torque adjustment. Such kind of oscillations, reported also by other researchers [8], [19], is a common issue of braking needed to be considered as it affects EV steerability and reduces energy recovery.

In Fig. 7, an improved Matlab®/Simulink® model is proposed. Block Drive-U provides direct torque control, power supply, and recuperation. Together with Drive-I, it arranges the torque stabilisation loop with PI current controller. Blocks Drive-T and Drive-W belong to the speed loop shredded in heavy braking. Gear and vehicle inertia are represented by the PLANT block. Load is applied to the motor shaft from the LOAD block together with TF. Torque Allocation, FLC, and Slip Processing are the parts of ECU shown in Fig. 2. In turn, the application torque signal *T* and vehicle velocity *v* feed back the Slip Processing block to reflect slipping friction (6) and air friction (4). Motor angular speed ω and torque T_M are used for recuperative power *P* calculation (8). Just like in [10], no climbing is applied.

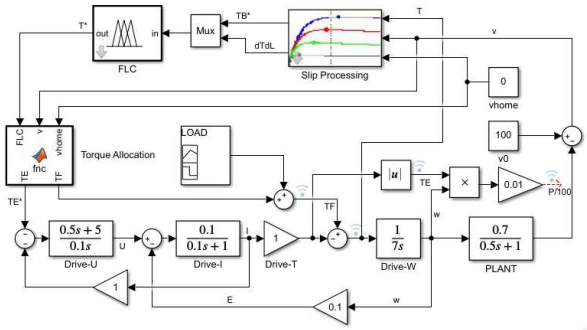

Fig. 7. Simulink model of the EV electric drive in the braking mode of operation.

As follows from Fig. 8, vehicle velocity (*v*, green) drops from v_0 = 100 km/h in 3 s.

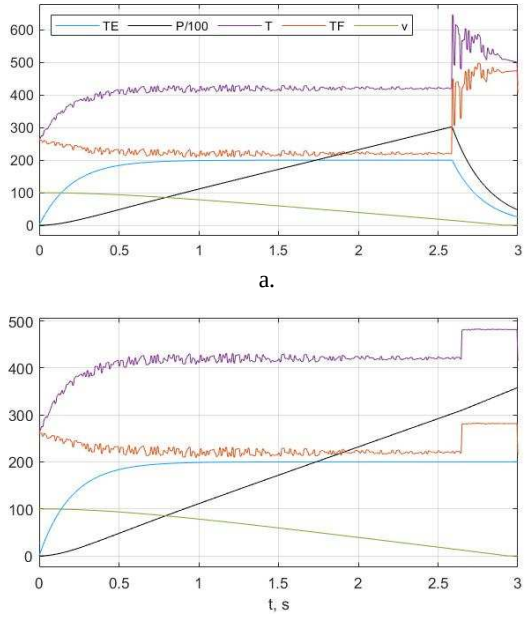

Fig. 8. Braking diagrams obtained from the Simulink model without EB (a) and with EB (b) at low velocity.

Total braking torque (*T*, purple) needed to ensure heavy stopping in response to driver's setpoint T_B^* = 420 Nm is obtained after allocation between motor (T_E, blue) and friction (T_F, orange) torque, wherein motor torque is restricted to 200 Nm. Torque oscillations are observed here mainly from FLC and reduce with velocity while converter switching is damped by the torque loop. In simulation, 100 Hz frequency was used for FLC processing at 200 Hz fundamental sample frequency. At low velocity v_{home} = 15 km/h, friction increases suddenly due to its static fraction. In Fig. 8 (a) EB turns off and

torque begins oscillate intensively. In contrast, in Fig. 8 (b) EB persist in this case, recuperation does not interrupt, and no additional torque chattering is detected on the motor shaft. Based on the power curve (*P*, black) and assuming 50% recuperative efficiency in (1), it turns out that nearly 22 kJ of energy is recovered during braking in the first case and 25 kJ – in the second one.

8. Conclusion

In the refined vehicle model, multiple factors are addressed, such as air resistance, road slope, and changeable friction. The improved motor and energy source model reflects the state of charge and electric current/voltage restrictions of the hybrid energy storage at various driving scenarios recognised by the tire model, such as smooth slowing and emergency antilock braking on different road surfaces. As a result, novel control arrangement is proposed, including fuzzy braking torque adjustment and stabilisation with torque allocation between electric and friction brakes thus integrating both friction and electric braking benefits. Obtained simulation diagram largely match the experimental curves. However, chattering of braking torque is reduced and evenly distributed throughout the braking process in the developed model.

References

[1] B. J. Varocky, Benchmarking of Regenerative Braking for a Fully Electric Car, Eindhoven University of Technology, Germany, 2011. 54 p.

[2] M. Shang, L. Chu, J. Guo and Y. Fang, "Hydraulic braking force compensation control for hybrid electric vehicles", International Conference on Computer, Mechatronics, Control and Electronic Engineering (CMCE), Changchun, China, 2010, pp. 335 – 339.

[3] S. M. Savaresi and M. Tanelli, Active Braking Control Systems Design for Vehicles, London: Springer, 2010, 254 p.

[4] S. Khastgir, "The simulation of a novel regenerative braking strategy on front axle for an unaltered mechanical braking system of a conventional vehicle converted into a hybrid vehicle", 8th International Conference and Exhibition on Ecological Vehicles and Renewable Energies (EVER), Monte Carlo, Monaco, 2013, pp. 1 – 6.

[5] F. Naseri, E. Farjah and T. Ghanbari, "An efficient regenerative braking system based on battery / supercapacitor for electric, hybrid, and plug-in hybrid electric vehicles with BLDC motor," IEEE Transactions on Vehicular Technology, v. 66, no 5, pp. 3724 – 3738. May 2017.

[6] Z. Chen, T. Lv, N. Guo, J. Shen, R. Xiao, X. Lu and Z. Yu, "Study on braking energy recovery efficiency of electric vehicles equipped with super capacitor," Chinese Automation Congress (CAC), Jinan, China, 2017, pp. 7231 – 7236.

[7] Y-B. Xie and S-C Wang, "Research on regenerative braking control strategy and Simulink simulation for 4WD electric vehicle", 2nd International Conference on Manufacturing Technologies (ICMT), Florence, USA, 2018, pp. 1 – 6.

[8] H. Lin and C. Song, "Design of a fuzzy logic controller for ABS of electric vehicle based on AMESim and Simulink," 2011 International Conference on Transportation, Mechanical, and Electrical Engineering (TMEE), Changchun, China, 2011, pp. 779 – 782.

[9] H. Jing, Z. Liu and J. Liu, "Wheel slip control for hybrid braking system of electric vehicle," International Conference on Transportation, Mechanical, and Electrical Engineering (TMEE), Changchun, China, 2011, pp. 743 – 746.

[10] A. Aksjonov, V. Vodovozov, K. Augsburg and E. Petlenkov, "Design of regenerative anti-lock braking system controller for 4 in-wheel-motor drive electric vehicle with road surface estimation," International Journal of Automotive Technology, vol. 19, no. 4, pp. 727 − 742, 2018.

[11] Brakes, Brake Control and Driver Assistance Systems: Function, Regulation and Components, K. Reif (Ed.), Friedrichshafen, Germany: Springer, 2014, 275 p.

[12] A. O. Kiyakli and H. Solmaz, "Modeling of an electric vehicle with MATLAB/Simulink," International Journal of Automotive Science and Technology, v. 2, no. 4, pp. 9 – 15, 2018.

[13] P. Spichartz, T. Bokker and C. Sourkounis, "Comparison of electric vehicles with single drive and four wheel drive system concerning regenerative braking," 12th International Conference on Ecological Vehicles and Renewable Energies (EVER), Monte-Carlo, Monaco, 2017, pp. 1 – 7.

[14] R. Pratap and A. Ruina, Introduction to Statics and Dynamics, Oxford University Press, 2002, 751 p.

[15] X. Zhang and H. Lin, "UAV anti-skid braking system simulation," 37th Chinese Control Conference, Wuhan, China, 2018, pp. 8453 – 8458.

[16] S. Kadowaki, K. Ohishi, T. Hata, N. Iida, M. Takagi, T. Sano and S. Yasukawa, "Antislip adhesion control based on speed sensorless vector control and disturbance observer for electric commuter train AT series 205-5000 of the east Japan railway company," IEEE Transactions on Industrial Electronics, vol. 54, no. 4, pp. 2001 – 2008, 2007.

[17] M. Cecotti, J. Larminie and B. Azzopardi, "Estimation of slip ratio and road characteristics by adding perturbation to the input torque," IEEE International Conference on Vehicular Electronics and Safety (ICVES), Istanbul, Turkey, 2012, pp. 31 – 36.

[18] H. Pacejka, Tyre and Vehicle Dynamics (3rd ed.), Oxford, UK: Butterworth–Heinemann, 2012, 672 p.

[19] M. Habibi and A. Yazdizadeh, "A novel fuzzy-sliding mode controller for antilock braking system," 2nd International Conference on Advanced Computer Control, v. 4, Shenyang, China, 2010, pp. 110 – 114.

[20] M. Cerdeira-Corujo, A. Costas, E. Delgado, A. Barreiro and A. Banos, "Gain-scheduled wheel slip reset control in automotive brake systems," International Symposium on Power Electronics, Electrical Drives, Automation and Motion (SPEEDAM), Anacapri, Italy, 2016, pp. 1255 – 1260.

[21] Y. Tao, X. Xie, H. Zhao, W. Xu and H. Chen, "A regenerative braking system for electric vehicle with four in-wheel motors based on fuzzy control," 36th Chinese Control Conference, Dalian, China, 2017, pp. 4288 – 4293.